

# Optical Regeneration at 40 Gb/s in Dispersion-Managed Transmission Lines With In-Line Synchronous Modulators

S. Waiyapot, S. K. Turitsyn, and V. K. Mezentsev

**Abstract**—Numerical optimization is performed of the 40-Gb/s dispersion-managed (DM) soliton transmission system with in-line synchronous intensity modulation. Stability of DM soliton transmission results from a combined action of dispersion, nonlinearity, in-line filtering, and modulation through effective periodic bandwidth management of carrier pulses. Therefore, analysis of the multiparametric problem is typically required. A two-stage time-saving numerical optimization procedure is applied. At the first step, the regions of the stable carrier propagation are determined using theoretical models available for DM solitons, and system parameters are optimized. At the second stage, full numerical simulations are undertaken in order to verify the tolerance of optimal transmission regimes. An approach developed demonstrates feasibility of error-free transmission over 20 000 km in a transmission line composed of standard fiber and dispersion compensation fiber at 40 Gb/s.

**Index Terms**—Dispersion-managed (DM) solitons, in-line filtering and modulation, optical regeneration, unlimited transmission over SMF at 40 Gb/s.

## I. INTRODUCTION

DISPERSION-MANAGED (DM) optical data transmission has become a mainstream in the development of high-speed communication systems [1]. DM soliton systems have significant advantages over classical soliton transmission lines: enhanced energy, resulting in higher signal-to-noise ratios (SNRs), reduced timing jitter, and strongly reduced nonlinear mixing between wavelength-division-multiplexed (WDM) signals [2]–[7]. Single-channel 40-Gb/s transmission over 10 000 km has also been reported in a DM line composed of dispersion-shifted fiber (DSF) and dispersion compensation fiber (DCF) [6]. However, in 40 Gb/s systems with strong dispersion management as in links based on standard fiber (SMF), DM return-to-zero (RZ) transmission is limited by intrachannel nonlinear effects and corresponding intersymbol interference (ISI) [8], [9].

Although in-line synchronous modulation requires periodic multiplexing/demultiplexing for WDM transmission, it will enable optical regeneration with reduced cost and complexity. It has been shown experimentally, that in a DM soliton system with weak dispersion management, in-line intensity modulation

(IM) can significantly improve the system performance. However, generalization of the IM technique for systems with strong dispersion management is not straightforward because of the large pulse broadening leading to bits overlapping and resulting into pattern-dependent nonlinear interactions. Moreover, the excess gain required to compensate for the loss due to modulation contributes to the additional buildup of noises in the zero time slots. Therefore, for strong dispersion management, where the dominant degradation results from the intrachannel nonlinear effects [8], [9], a simultaneous stabilization is required of the timing and amplitude jitters of bit-carrier pulses (marks) and suppression of the growing ghost pulses and the background noise in zero time slots (spaces).

In the DM line, the efficiency of conventional modulation is significantly decreased, compared with classical soliton-based transmission system [15], [16]. In order to recover the efficiency of the control, it has been proposed to use a periodic enhancement of system nonlinearity by means of extra amplification at regeneration sites to convert the DM pulse into classical soliton through the technique called “black box” optical regeneration (BBOR) [15], [16]. The benefit of DM soliton to fundamental soliton conversion is that the stabilization of a conventional soliton is more efficient compared to a DM soliton.

Recently, it has been proposed to enhance nonlinearity in the BBOR technique by the use of highly nonlinear fiber (HNF) at the modulator location [17]–[19]. Note that the HNF has already been extensively used for wavelength conversion [20], [21]. First numerical results demonstrating 40-Gb/s transmission over 20 000 km of SMF using modified modulation technique have been reported in [17]–[19]. However, comprehensive investigation of the stable regimes in multidimensional parameter space is limited by the computational time required for a single optimization run. New effective approaches are then highly desirable for further system optimization. The combined action of the filters, modulators, and the HNF can provide an effective management of the carrier pulse bandwidth. The nonlinearly enhanced modulation keeps the benefits of the conventional modulator in reducing the timing jitter and also utilizes the nonlinearity for efficient filtering. This makes possible the pulse stabilization while keeping the pulse width narrow enough so that the excess gain introduced by modulators is not too high.

In this paper, the bandwidth management technique is advanced further. An important difference compared with previous work is that the analysis is limited to the case of the periodically recovered carrier only, gaining instead a possibility of

Manuscript received June 7, 2002; revised September 16, 2002. This work was supported by the Engineering and Physical Sciences Research Council (U.K.).

The authors are with the Photonics Research Group, Electronic Engineering Department, Aston University, Birmingham B4 7ET, U.K. (e-mail: suttawaw@aston.ac.uk).

Digital Object Identifier 10.1109/JLT.2002.806750

the advanced optimization procedure. Taking advantage of the simple semitheoretical methods well developed for DM solitons, the system and input pulse parameters are optimized before applying full numerical modeling. The linear stability analysis based on the variational approach [22], [23], [27] has been successfully used to investigate DM soliton transmission [12], [13], [24]–[26]. The advantage of the method is a capability to predict both timing and energy fluctuations of the carrier pulse and the growth of the background noise in the zero time slots. At first glance, this method might not look appropriate for the 40-Gb/s systems with strong overlapping of bits, since it is based on consideration of the single-pulse propagation only. However, as is justified subsequently, the linear stability analysis is still a surprisingly useful method, suitable for investigation of high-bit-rate systems.

In the present work, an optimization of transmission lines is performed, similar to that considered in [18], [19], applying the stability analysis at the first stage. This allows us to extend analysis well beyond the previously considered region of parameters. A two-step time-saving numerical optimization procedure is applied. At the first stage, the regions of stable carrier propagation are determined, and system parameters are optimized. At the second stage, the full numerical simulations are applied in order to verify tolerance of the optimal transmission regimes.

To demonstrate the advantages of the method and to point out its limitations, a comparison was performed of the transmission at 10 Gb/s and 40 Gb/s in the case of weak dispersion management. Then, the limitations of using a conventional modulator in a strong DM line at 40 Gb/s are analyzed. The superiority is confirmed of the modified synchronous modulation over conventional modulation technique for lines with strong dispersion management. Taking advantage of the time-saving numerical approach, the regimes of stable transmission are identified and the optimal system characteristics are determined in the multi-dimensional parameter space. Finally, the results are verified by direct numerical modeling.

## II. THEORY

The signal transmission down the fiber line can be modeled by the modified nonlinear Schrödinger equation (NLSE) (written here in the normalized units)

$$i \frac{\partial q}{\partial z} + \frac{D(z)}{2} \frac{\partial^2 q}{\partial t^2} + s(z)|q|^2 q = -i\Gamma(z)q \quad (1)$$

where the variables  $z$ ,  $t$ ,  $|q|^2$ ,  $D(z)$ ,  $s(z)$ , and  $\Gamma(z)$  are the distance, retarded time, power, fiber dispersion, fiber nonlinear coefficient, and fiber loss normalized by  $2\pi c t_0^2 / \lambda^2 D_0$ ,  $t_0$ ,  $P_0$ ,  $D_0$ ,  $(4\pi^2 c n_2 t_0^2 P_0) / \lambda^3 A_{\text{eff}} D_0$ , and  $10\lambda^2 D_0 / (\pi c t_0^2 \ln 10)$ , respectively. Here  $t_0$ ,  $D_0$ , and  $P_0$  are arbitrarily chosen references for the time, dispersion, and power, respectively. In the present analysis, the carrier pulse is assumed to have the Gaussian profile characterized by six parameters, as follows:

$$q = A \exp \left[ - \left( \frac{1}{2\tau^2} + iC \right) (t - \xi)^2 - i\kappa(t - \xi) + i\theta \right]. \quad (2)$$

Here,  $A(z)$ ,  $\tau(z)$ ,  $C(z)$ ,  $\kappa(z)$ ,  $\xi(z)$ , and  $\theta(z)$  are the amplitude, width, chirp, frequency, temporal position, and phase of the pulse, respectively. It should be noted that the pulse shape of

the true periodic solution of (1) is not always given accurately by the Gaussian approximation. However, this approach gives very reasonable simple approximation of the DM soliton evolution. More details on validation of the Gaussian approximation and more accurate analysis can be found in [23], [27]. The evolution of the pulse parameters along the fiber line is then approximated by a set of coupled ordinary differential equations derived using either a variational approach or the root-mean-square momentum method [to simplify the notation, we will use  $D$ ,  $s$ , and  $\Gamma$  instead of  $D(z)$ ,  $s(z)$ , and  $\Gamma(z)$ ], as follows:

$$\frac{dA}{dz} = DAC \quad (3a)$$

$$\frac{d\tau}{dz} = -2D\tau C \quad (3b)$$

$$\frac{dC}{dz} = \frac{sA^2}{2\sqrt{2}\tau^2} \exp(-2\Gamma z) - \frac{D}{2\tau^4} + 2DC^2 \quad (3c)$$

$$\frac{d\kappa}{dz} = 0 \quad (3d)$$

$$\frac{d\xi}{dz} = -D\kappa \quad (3e)$$

where the dispersion parameter  $D$  has a positive or negative sign in the fiber segments with anomalous and normal dispersion, respectively. Transfer functions of the filter and modulator are approximated in this section by the Gaussian functions  $\exp[-\beta\omega^2]$  and  $\exp[-\mu t^2]$  in the frequency and time domain, respectively. The modulator function approximates one cycle of a sinusoidal function centered at  $t = 0$ . The filter transforms the Gaussian pulse parameters as follows:

$$A_{\text{out}} = \frac{A_{\text{in}}}{[(1 + 2\beta/\tau_{\text{in}}^2)^2 + 16\beta^2 C_{\text{in}}^2]^{1/4}} \times \exp \left[ - \frac{\beta\tau_{\text{in}}^2 \kappa_{\text{in}}^2}{\tau_{\text{in}}^2 + 2\beta(1 + 4\tau_{\text{in}}^4 C_{\text{in}}^2)} \right] \quad (4a)$$

$$\tau_{\text{out}}^2 = \frac{(\tau_{\text{in}}^2 + 2\beta)^2 + 16\beta^2 \tau_{\text{in}}^4 C_{\text{in}}^2}{\tau_{\text{in}}^2 + 2\beta(1 + 4\tau_{\text{in}}^4 C_{\text{in}}^2)} \quad (4b)$$

$$C_{\text{out}} = \frac{\tau_{\text{in}}^4 C_{\text{in}}}{(\tau_{\text{in}}^2 + 2\beta)^2 + 16\beta^2 \tau_{\text{in}}^4 C_{\text{in}}^2} \quad (4c)$$

$$\kappa_{\text{out}} = \frac{\tau_{\text{in}}^2 \kappa_{\text{in}}}{\tau_{\text{in}}^2 + 2\beta(1 + 4\tau_{\text{in}}^4 C_{\text{in}}^2)} \quad (4d)$$

$$\xi_{\text{out}} = \xi_{\text{in}} - \frac{4\beta\tau_{\text{in}}^4 C_{\text{in}} \kappa_{\text{in}}}{\tau_{\text{in}}^2 + 2\beta(1 + 4\tau_{\text{in}}^4 C_{\text{in}}^2)}. \quad (4e)$$

The modulator transfer function gives

$$A_{\text{out}} = A_{\text{in}} \exp \left[ - \frac{\mu \xi_{\text{in}}^2}{1 + 2\mu\tau_{\text{in}}^2} \right] \quad (5a)$$

$$\tau_{\text{out}}^2 = \frac{\tau_{\text{in}}^2}{1 + 2\mu\tau_{\text{in}}^2} \quad (5b)$$

$$C_{\text{out}} = C_{\text{in}} \quad (5c)$$

$$\kappa_{\text{out}} = \kappa_{\text{in}} - \frac{4\mu C_{\text{in}} \tau_{\text{in}}^2}{1 + 2\mu\tau_{\text{in}}^2} \xi_{\text{in}} \quad (5d)$$

$$\xi_{\text{out}} = \frac{\xi_{\text{in}}}{1 + 2\mu\tau_{\text{in}}^2}. \quad (5e)$$

The subscripts in and out correspond to the pulse parameters at the input and the output of modulator and filter, respectively. We use an iterative shooting method to find fixed-point solutions of (3)–(5) whose amplitude, width, chirp, frequency, and position are completely recovered after one periodic section. Next, the equations are linearized around the periodic solution. The evolution of the perturbations of the pulse parameters in the fiber is governed by

$$\frac{d\Delta A}{dz} = D(C_0\Delta A + A_0\Delta C) \quad (6a)$$

$$\frac{d\Delta\tau}{dz} = -2D(C_0\Delta\tau + \tau_0\Delta C) \quad (6b)$$

$$\frac{d\Delta C}{dz} = \frac{sA_0^2}{\sqrt{2}\tau_0^2} \left[ \frac{\Delta A}{A_0} - \frac{\Delta\tau}{\tau_0} \right] \exp(-2\Gamma z) + \frac{2D}{\tau_0^5} \Delta\tau + 4DC_0\Delta C \quad (6c)$$

$$\frac{d\Delta\kappa}{dz} = 0 \quad (6d)$$

$$\frac{d\Delta\xi}{dz} = -D\Delta\kappa. \quad (6e)$$

Here, the quantities with subscript 0 correspond to the periodic pulse parameters. We also linearize the transfer function of filter and modulator in (4) and (5), assuming small perturbations of the pulse parameters, resulting in the equations given in the Appendix. Note that the linear fluctuations of amplitude, width, and chirp are decoupled from the perturbations of the frequency and temporal positions, as follows:

$$\begin{bmatrix} \Delta A_{n+1} \\ \Delta\tau_{n+1} \\ \Delta C_{n+1} \end{bmatrix} = \begin{bmatrix} H_{11} & H_{12} & H_{13} \\ H_{21} & H_{22} & H_{23} \\ H_{31} & H_{32} & H_{33} \end{bmatrix} \begin{bmatrix} \Delta A_n \\ \Delta\tau_n \\ \Delta C_n \end{bmatrix} \quad (7a)$$

$$\begin{bmatrix} \Delta\kappa_{n+1} \\ \Delta\xi_{n+1} \end{bmatrix} = \begin{bmatrix} K_{11} & K_{12} \\ K_{21} & K_{22} \end{bmatrix} \begin{bmatrix} \Delta\kappa_n \\ \Delta\xi_n \end{bmatrix}. \quad (7b)$$

In order to perform a stability analysis, the eigenvalues of the transfer matrix  $H$  and  $K$  in (7) are to be determined. Note that  $H$  and  $K$  govern evolution of the linear perturbations. The maximum absolute value of the three eigenvalues  $\lambda_i$  ( $i = 1 - 3$ ) of the matrix  $H$  determine the stability properties. A quantity  $P = [\max(|\lambda_1|, |\lambda_2|, |\lambda_3|) - 1]$  is called a stability index hereafter. It is considered as a stability indicator showing either the increment of instability or the decrement of the decay of the pulse energy perturbations in the stable case. Obviously, linear perturbations decrease if  $P$  is negative and increase if  $P$  is positive. In a similar manner, we can introduce a stability index of the pulse timing position given by the eigenvalues of the matrix  $K$ . Stability of spaces can be determined by the similar analysis of the background evolution. Following [24], we neglect the fiber nonlinearity and find the solution of the lowest order linear mode in one periodic section. The growth of linear mode can be defined as  $\gamma = A_{\text{out}}/A_{\text{in}}$ , where  $A_{\text{in}}$  and  $A_{\text{out}}$  correspond to the amplitude of linear mode at beginning and end of one periodic section, respectively. In this paper, we use  $\gamma - 1$  to determine the stability index for space. Thus, in our analysis, we consider the stability of the energy and timing position of the bit-carrier pulse (mark) and the stability of the background

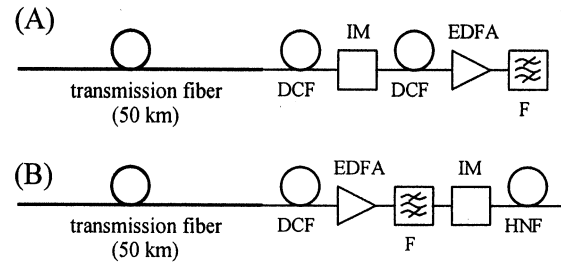


Fig. 1. Scheme of the considered systems. (A) With conventional modulator. (B) With modified modulator enhanced by HNF.

in zero time slot (space). Negative values for any index mean stability, whereas positive values correspond to instability. The larger negative indexes can then be interpreted as the larger stability margin.

### III. SYSTEM CONFIGURATION AND PARAMETERS

Two sample configurations of the transmission system considered in this paper are depicted in Fig. 1. System (A) or system with conventional modulation composes of transmission fiber, DCF, filter, intensity modulator and amplifier while system (B) or system with modified modulation composes of the same components as system (A) but has additional HNF fiber at the modulation site.

The transmission fiber of 50 km length is either DSF with dispersion  $d = 1$  ps/km/nm, dispersion slope  $d'' = 0.06$  ps/nm<sup>2</sup>/km, loss  $\alpha = 0.21$  dB/km, and effective area  $A_{\text{eff}} = 55 \mu\text{m}^2$ , or SMF with  $d = 17$  ps/km/nm,  $d'' = 0.06$  ps/nm<sup>2</sup>/km,  $\alpha = 0.21$  dB/km, and  $A_{\text{eff}} = 80 \mu\text{m}^2$ . The DCF used in simulations has  $d = -80$  ps/nm/km,  $d'' = -0.2$  ps/nm<sup>2</sup>/km,  $\alpha = 0.5$  dB/km, and  $A_{\text{eff}} = 26 \mu\text{m}^2$ . The length of DCF is adjusted to provide residual dispersion around zero. As nonlinear fiber, we considered the HNF with  $d = 1.8$  ps/nm/km,  $d'' = 0.03$  ps/nm<sup>2</sup>/km,  $\alpha = 0.5$  dB/km, and nonlinear coefficient  $n_2/A_{\text{eff}} = 2 \times 10^{-9}$  W<sup>-1</sup>. The erbium-doped fiber amplifier (EDFA) with a noise figure of 6 dB is installed after the DCF for both systems. The synchronous intensity modulator is inserted every fourth map period inside the segment DCF in scheme A and at the end of the segment DCF in scheme B. The modulation depth is 0.1. The gain of the amplifier at fourth map period in system B also compensates for the loss introduced by the HNF and boosts up the energy for the conversion of the DM pulse to soliton pulse. The in-line filter with bandwidth of 3.0 nm (at 10 Gb/s) and 1.5 nm (at 40 Gb/s) are installed after the amplifier for both systems.

### IV. RESULTS OF NUMERICAL MODELING AND DISCUSSION

We first apply stability analysis to the DM line with a weak map strength operating at 10 Gb/s and 40 Gb/s in order to validate the accuracy of the stability analysis for different transmission regimes. Here, the DSF is used as a transmission fiber; the average dispersion is 0.05 ps/nm/km, and the pulse energy is 0.15 pJ. Fig. 2 presents the stability analysis results. Stability indexes of (a) energy, (b) timing, and (c) space are shown versus the modulator location in DCF. Solid and dotted lines correspond to 10 Gb/s and 40 Gb/s, respectively.

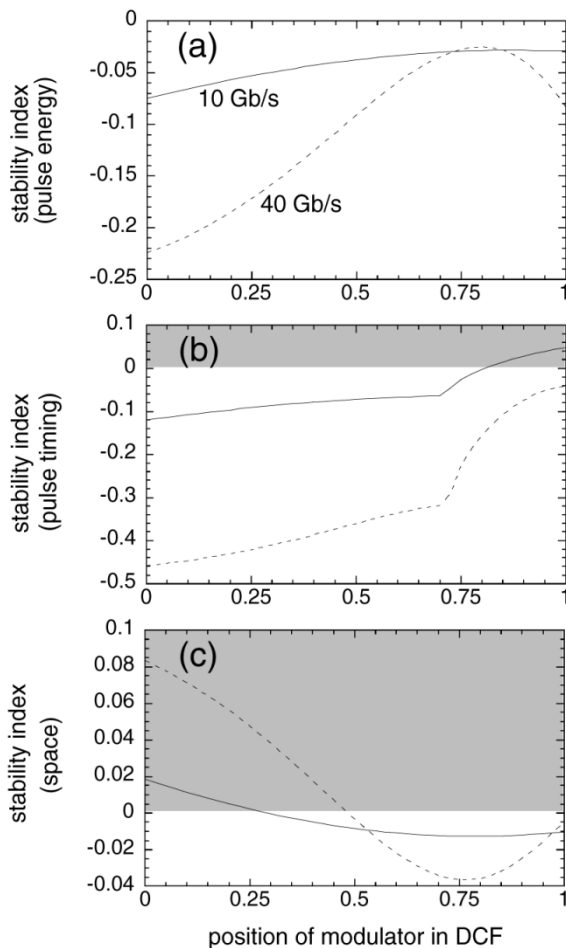


Fig. 2. Stability index of (a) energy, (b) timing position, and (c) space versus the modulator location in DCF for system based on DSF/DCF. Solid and dotted lines correspond to 10 Gb/s and 40 Gb/s, respectively. The pulse energy is 0.15 pJ.

Results presented in Fig. 2 can be understood in the following way. The effect of the modulator is stronger when the pulsewidth at the modulator location is larger (as it is for 40 Gb/s), thus leading to stronger stabilization in pulse energy and timing. The chirp at the modulator can also affect the stability of pulse timing. Improper chirp at the modulator can make positive feedback, leading to the rise of the time shift of the pulse [12], [13]. Note that the stability analysis presented in Fig. 2 is based on the single-carrier propagation; therefore, comparison of the results for different bit rates is not straightforward here.

It is well known that in 40-Gb/s systems, the nonlinear interaction of the overlapping pulses can substantially degrade the system performance. We also use a stronger modulator and filter in 40-Gb/s systems, and this results in better stability compared with the 10-Gb/s case. However, a stronger filter makes it easy to build up background noise in the zero time slots. Predictions of the linear stability analysis have been verified in the direct numerical simulations, as shown in Fig. 3. Fig. 3 depicts  $Q$ -factor evolution along the line for different locations of the IM within the DCF. The  $Q$ -factors in this figure and throughout the paper are obtained by the average of a set of simulations with a 128 pseudorandom bit sequences (PRBSs) and three different

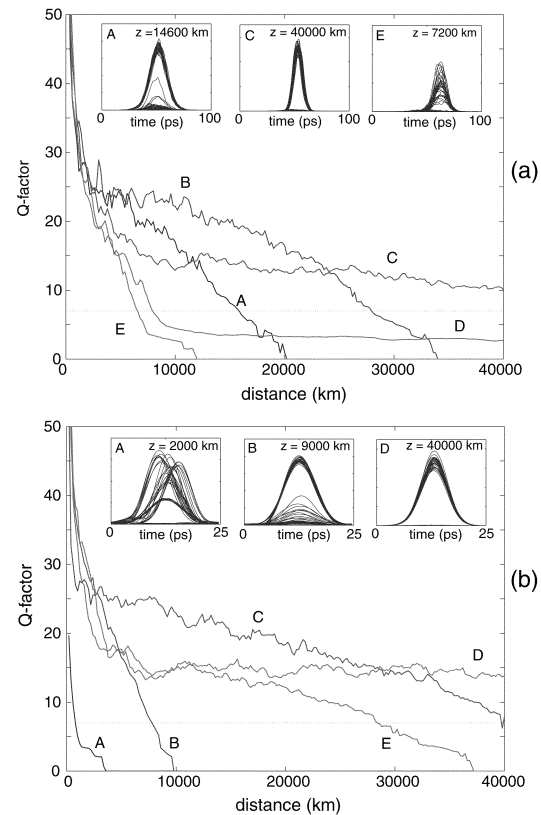


Fig. 3. Evolution of  $Q$ -factor along the DSF/DCF transmission line at (a) 10 Gb/s and (b) 40 Gb/s. Different curves correspond to the following locations of the in-line modulator: A—beginning of DCF; B—0.25 DCF; C—0.5 DCF; D—0.75 DCF; E—end of DCF. Insets show the eye diagrams after some transmission distances for different locations of the modulator within DCF.

noise seeds. The amplified spontaneous-emission noise spectrum is white over the considered spectral interval. The probability density function for the noise is assumed to be Gaussian distribution.

In the case of the 10-Gb/s transmission [Fig. 3(a)], the results of the numerical modeling of NLSE, in general, are in agreement with the results of the linear stability analysis presented in Fig. 2. Eye diagrams show that the buildup of noise and timing shift leads to the signal degradation. Note that even if some points of IM location are formally stable, the linear stability with small negative indexes cannot guarantee stable transmission over unlimited distances. Fig. 3(b) shows the evolution of the  $Q$ -factor with distance in a 40-Gb/s system obtained by direct numerical modeling. Eye-diagrams indicate that, in the case of position A, timing jitter causes the main problems. It is also seen that in the case of position B, the buildup of the background noise in the zero time slots is the main limiting factor. Because the linear stability analysis neglects the effects of pulse interaction, the predictions may not be correct when the interaction is the main limiting factor. For instance, in the case of position A, the system is degraded by frequency shift from the nonlinear interaction, but not by the growing background in space. Therefore, there are evident limitations on the application of the stability analysis in the case of strong ISI. However, for DSF/DCF based lines at 40 Gb/s, as it is shown in Figs. 4 and 5, predictions of the

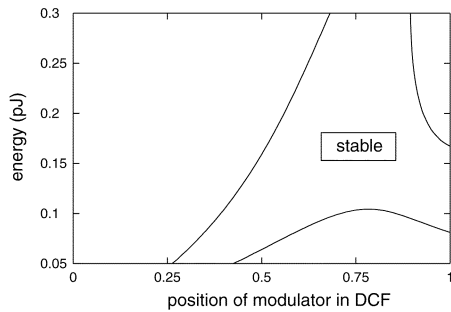


Fig. 4. Stability region defined as the area where all three indexes are negative in the plane (energy and location of the modulator in DCF) for DSF/DCF transmission system.

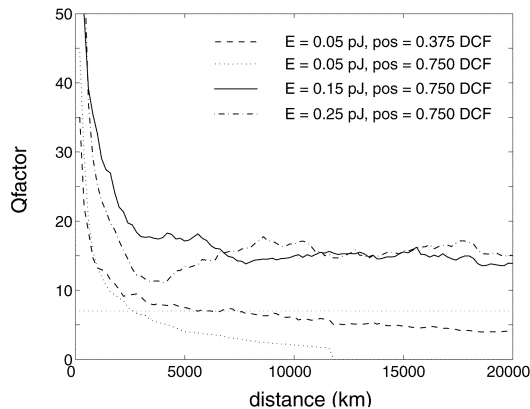


Fig. 5. Evolution of  $Q$ -factor for the same system as in Fig. 4. Different curves correspond to different locations of the in-line modulator and pulse energy as indicated in the inset.

stability analysis (Fig. 4) are in very good agreement with the results of the direct modeling (Fig. 5). This is because the map strength in such systems is not too large, even for a 40-Gb/s bit rate.

Next, we consider the 40-Gb/s transmission with strong dispersion management. Note that for strong dispersion management, it is not always possible to find DM soliton with a small enough width. The pulse broadening inherent for strong management, combined with the modulator action, causes the energy leakage into other slots.

We vary the dispersion of transmission fiber, denoted by DF, in the range of 0.5–20 ps/nm/km. The other transmission fiber parameters are based on the DSF model. We consider the transmission system A with average dispersion of 0.05 ps/nm/km and system B with a span average dispersion of 0 ps/nm/km. The span average dispersion value for system B is exclusive of the HNF. In systems using strong dispersion management at 40 Gb/s stable transmission can hardly be achieved in the conventional schemes with filtering and in-line modulation, as it can be seen from Fig. 6. As a matter of fact, this is an example when nonlinearity plays a positive role and is required to stabilize transmission.

Increase of the effective nonlinearity can be achieved either by using the extra EDFA at the IM location or by utilization of the HNF. Insertion of the HNF helps both to compress the carrier pulse and to enhance efficiency of the filtering. Fig. 6 clearly shows a substantial improvement of the stability indexes with introduction of the HNF in a strong dispersion management

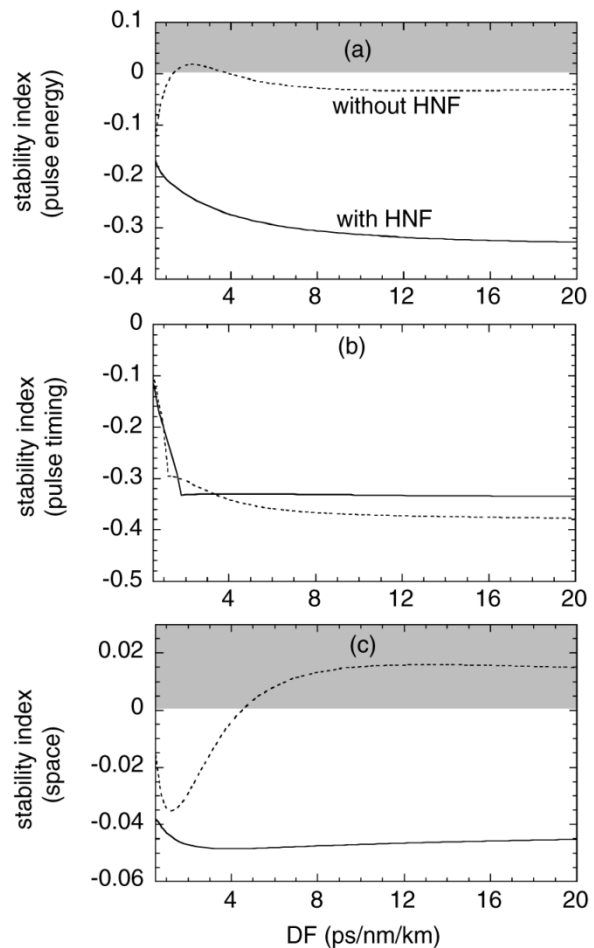


Fig. 6. Stability index of (a) energy, (b) timing, and (c) space versus dispersion of the transmission fiber for the line with (solid line) and without (dotted line) HNF. The pulse energy is 0.11 pJ for both cases.

system. Direct simulations of the pattern propagation (Fig. 7) also demonstrate significant suppression of the ghost pulses in the zero time slots and stabilization of ones by means of the HNF.

These results indicate that stable transmission at 40 Gb/s in SMF/DCF systems is feasible with an appropriate use of the HNF. The stability analysis can help to find optimal transmission regimes. From here throughout the paper, we focus on the transmission system B based on the SMF with the modified modulator enhanced by the HNF. The length of the HNF is typically around 10 km.

It has already been observed in [18] that the modulator location before the HNF is advantageous because, in this case, pulse tails are suppressed by the modulator before entering the HNF. This leads to corresponding suppression of the pulse-to-pulse interaction. Figs. 8 (stability analysis) and 9 (direct single simulations of the eye diagrams) confirm this result and show that the main advantage in using IM before HNF is an improvement of the pulse timing position stability.

It is important that, applying linear stability analysis, we can easily optimize two and more parameters simultaneously, which is rather difficult using full numerical modeling. Figs. 10–12 show a summary of the stability analysis in the plane of two parameters: “DF (transmission fiber dispersion), span average

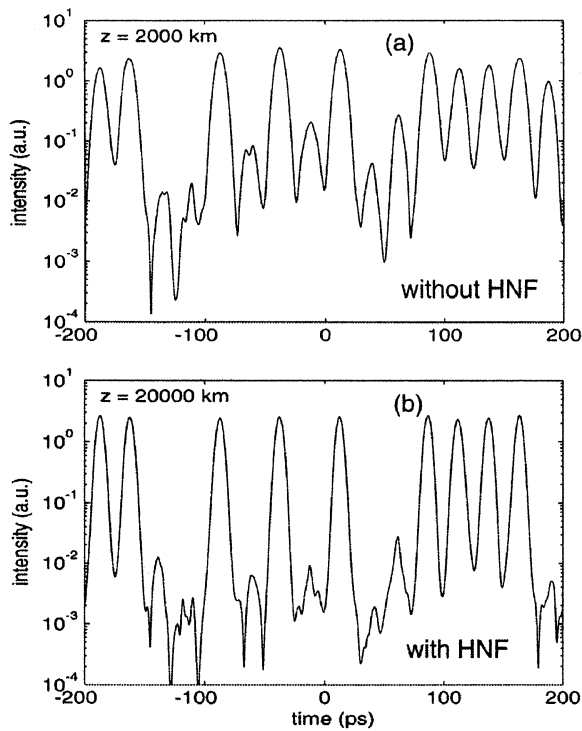


Fig. 7. Suppression of the ghost pulses by the HNF. Signal power is shown after propagation in system without HNF (a) (after 2000 km) and with HNF (b) (after 20 000 km). The parameters are same as in Fig. 6 with  $DF = 17$  ps/nm/km. The input signals are [1 100 101 010 011 110].

dispersion” in Fig. 10; “pulse energy, span average dispersion” in Fig. 11; and “pulse energy, length of HNF” in Fig. 12. Recall that in the stability region, all three indexes are negative. Note again that the span average dispersion is excluding of the HNF. Fig. 10 shows that, with the HNF, stability can be achieved for high enough dispersion of the transmission fiber if the overall average dispersion (inclusive of the HNF) is kept in a certain range. In the simulations presented in Fig. 11 a stable regime has been achieved by changing the length of the DCF (or changing span average dispersion) and the soliton energy. We found that the largest negative value of the energy stability index is at the zero average dispersion and for the energy of about 0.11 pJ. Performed optimization demonstrates that under certain conditions, the stabilization effect can surpass the signal degradation.

Fig. 12 shows the stability region in the plane of “pulse energy, length of HNF.” We also use here for comparison another set of HNF parameters—HNF2, which is commercially used in wavelength conversion [21] to verify how results are sensitive to a particular realization of HNF. HNF2 has  $d = 0.2$  ps/nm/km,  $d'' = 0.03$  ps/nm<sup>2</sup>/km,  $\alpha = 0.5$  dB/km, and higher nonlinear coefficient  $n_2/A_{\text{eff}} = 4.16 \times 10^{-9}$  W<sup>-1</sup>. It can be seen that the lower energy is required when the length of HNF is increasing or equivalent when the fiber is more nonlinear. This again means that stabilization of the transmission is possible only when a certain overall nonlinearity is incorporated into the system. The span average dispersion for a system with the HNF and HNF2 are zero and 0.08 ps/nm/km, respectively. It is important that the overall average dispersion (inclusive of HNF) should have an adequately small amount of anomalous dispersion to support soliton propagation. Thus, we set the span average dispersion of

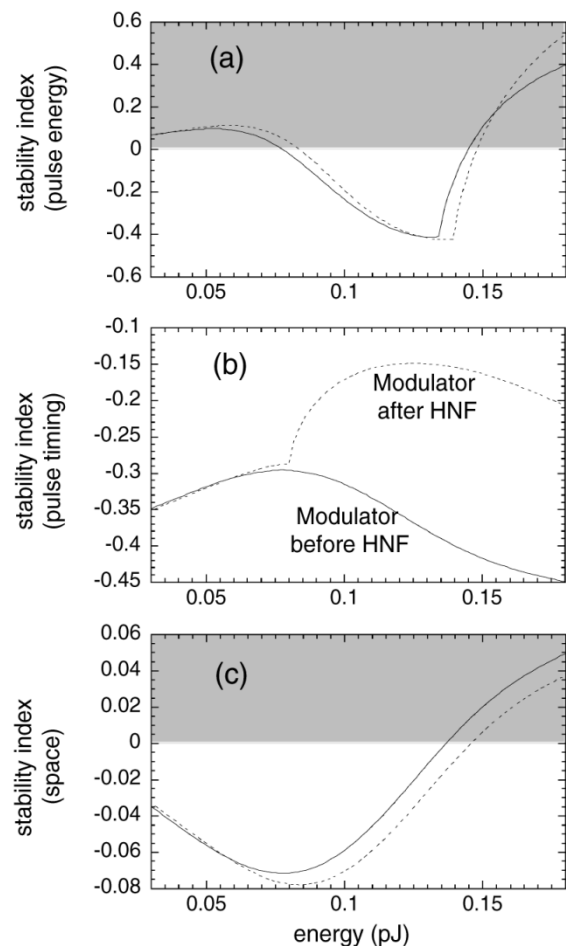


Fig. 8. Stability index of (a) energy, (b) timing, and (c) space versus pulse energy in the system with modulator before HNF (solid line) and modulator after HNF (dotted line). The span average dispersion is zero.

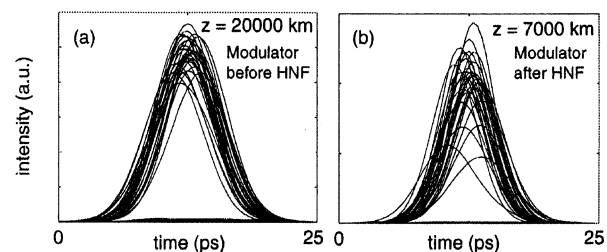


Fig. 9. Eye diagrams of a 128 PRBS in the system with modulator (a) before and (b) after HNF. The pulse energy is 0.11 pJ.

a system with HNF2 slightly higher than a system with the HNF because of the smaller local dispersion in HNF2.

The applied approach allows us to identify regions of stability within reasonably short computational time which is important for massive optimization involving more than two parameters to be optimized. Note that, in agreement with [18] and [19] (where time-consuming direct modeling has been applied), our method shows that the regeneration can be expected around the point of zero span average dispersion. As the span average dispersion deviates from the zero value, a power margin decreases. This means, in particular, that using direct numerical optimization, one should choose a relatively small step in signal power to register such stable transmission regimes. To validate the results

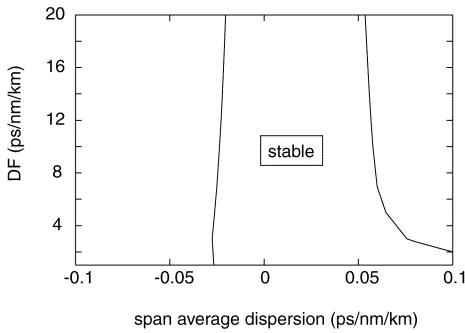


Fig. 10. Stability region in the plane "DF, span average dispersion" for transmission system with HNF. The pulse energy is 0.11 pJ.

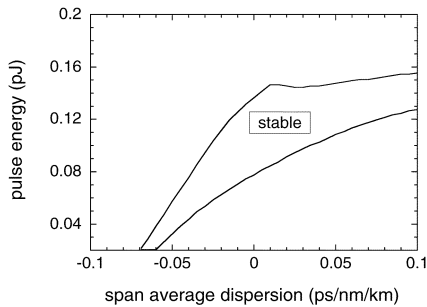


Fig. 11. Stability region in the plane "pulse energy, span average dispersion" for SMF/DCF transmission system with HNF.

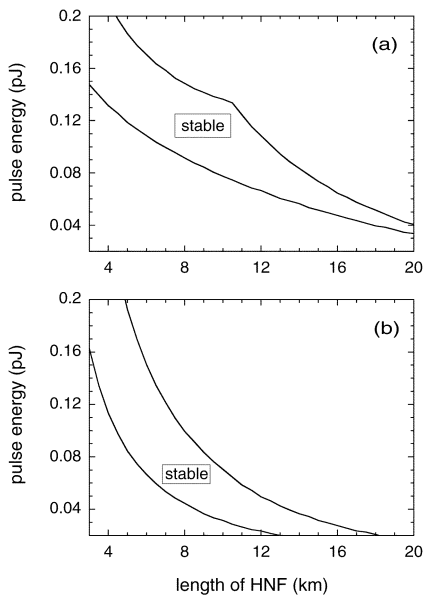


Fig. 12. Stability region in the plane "pulse energy, HNF length" for SMF/DCF transmission system exploiting (a) HNF and (b) commercial HNF2. The span average dispersion for systems with HNF and HNF2 are zero and 0.08 ps/nm/km, respectively.

of the stability analysis, next we applied direct numerical modeling around the found optimal regions of parameters. Fig. 13 presents  $Q$ -factor evolution for different studied systems: with SMF/DCF with and without HNF. The pulse energy is 0.11 pJ. The length of HNF and HNF2 are 10 and 6 km, respectively. The average dispersion for a system without HNF is 0.05 ps/nm/km. The span average dispersion for systems with HNF and HNF2 are zero and 0.08 ps/nm/km, respectively. This makes the overall

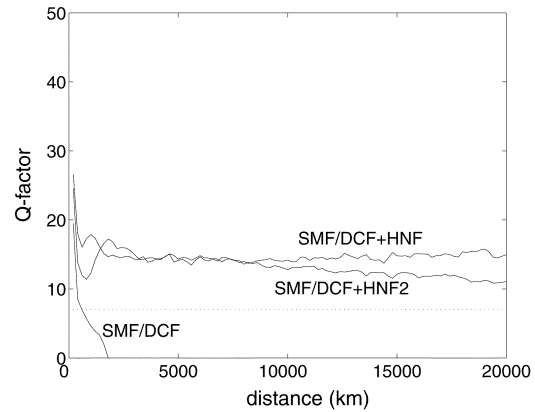


Fig. 13. Direct numerical modeling of SMF/DCF and SMF/DCF+HNF lines with in-line modulator.

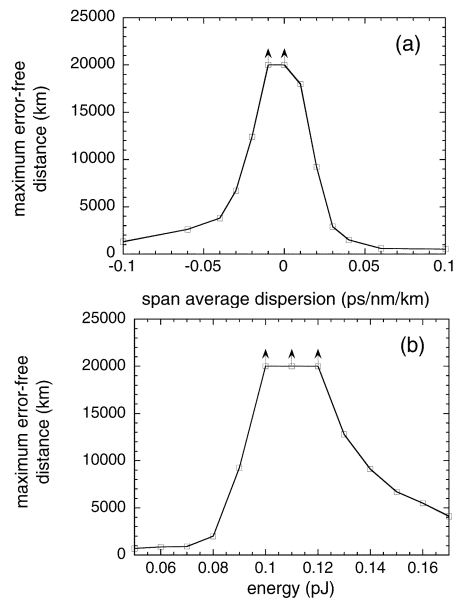


Fig. 14. Tolerance of the transmission against variations of the input pulse energy for SMF/DCF system with HNF. Here, the length of HNF is 10 km. (a) Energy is 0.11 pJ. (b) Span average dispersion is zero.

average dispersion for systems with HNF and HNF2 are about 0.071 and 0.083 ps/nm/km, respectively. It is seen from Fig. 13 that the results of direct modeling are in a good agreement with the stability analysis.

Stabilization of the  $Q$ -factor clearly indicates regeneration of the optical signal in accordance with the stability analysis predictions. Note that there is no big difference in transmission between using both types of HNF. Fig. 14 shows the results of direct numerical simulations of the tolerance against variations of the input pulse energy and the average dispersion for the previously described regeneration regime. The error-free distance is the distance in which the  $Q$ -factor is more than 7. This figure indicates that the input signal with the energy below a certain threshold is not regenerated because the carrier energy is not large enough for the conversion into fundamental soliton.

## V. CONCLUSION

We have presented an efficient and time-saving optimization technique capable of predicting optical regeneration regimes

in 40-Gb/s systems. We applied a two-stage procedure to determine optimal transmission regime. At the first step, we described regions of stable carrier propagation, using stability analysis available for DM solitons. On the second stage, we applied direct numerical modeling and investigated tolerance of optimal transmission regimes. We considered systems with conventional and modified modulation enhanced by HNF. In the case of strong dispersion management, the modified modulator demonstrates superior properties compared with the conventional modulation technique. We also discussed the limitations of the stability analysis in the systems with strong nonlinear interaction. However, as it is shown here, linear analysis is still a surprisingly useful method to investigate such systems. We would like to point out that the applied simple numerical approach is especially efficient for multiparametric optimization. The developed approach allows us to demonstrate feasibility of error-free transmission over 20 000 km of SMF/DCF at 40 Gb/s.

#### APPENDIX

The filter transfer function (4a)–(4e) are linearized in terms of the small fluctuations in the pulse parameters as

$$\Delta A_{\text{out}} = h_{11}\Delta A_{\text{in}} + h_{12}\Delta\tau_{\text{in}} + h_{13}\Delta C_{\text{in}} \quad (\text{A1a})$$

$$\Delta\tau_{\text{out}} = h_{21}\Delta A_{\text{in}} + h_{22}\Delta\tau_{\text{in}} + h_{23}\Delta C_{\text{in}} \quad (\text{A1b})$$

$$\Delta C_{\text{out}} = h_{31}\Delta A_{\text{in}} + h_{32}\Delta\tau_{\text{in}} + h_{33}\Delta C_{\text{in}} \quad (\text{A1c})$$

$$\Delta\kappa_{\text{out}} = k_{11}\Delta\kappa_{\text{in}} + k_{12}\Delta\xi_{\text{in}} \quad (\text{A1d})$$

$$\Delta\xi_{\text{out}} = k_{21}\Delta\kappa_{\text{in}} + k_{22}\Delta\xi_{\text{in}}. \quad (\text{A1e})$$

The coefficients appearing in (A1a)–(A1e) are given as

$$h_{11} = F_1^{-1/4} \quad (\text{A2a})$$

$$h_{12} = 2\beta F_1^{-5/4} A_{\text{in},0}(2\beta + \tau_{\text{in},0}^2)/\tau_{\text{in},0}^5 \quad (\text{A2b})$$

$$h_{13} = -8\beta^2 F_1^{-5/4} A_{\text{in},0} C_{\text{in},0} \quad (\text{A2c})$$

$$h_{21} = 0 \quad (\text{A2d})$$

$$h_{22} = F_2\tau_{\text{in},0}/(F_3^{3/2}F_4^{1/2}) \quad (\text{A2e})$$

$$h_{23} = -8\beta(2\beta + \tau_{\text{in},0}^2)\tau_{\text{in},0}^6 C_{\text{in},0}/(F_3^{3/2}F_4^{1/2}) \quad (\text{A2f})$$

$$h_{31} = 0 \quad (\text{A2g})$$

$$h_{32} = 8\beta(2\beta + \tau_{\text{in},0}^2)\tau_{\text{in},0}^3 C_{\text{in},0}/F_4^2 \quad (\text{A2h})$$

$$h_{33} = F_2\tau_{\text{in},0}^4/F_4^2 \quad (\text{A2i})$$

$$k_{11} = \tau_{\text{in},0}^2/F_3 \quad (\text{A2j})$$

$$k_{12} = 0 \quad (\text{A2k})$$

$$k_{21} = -4\beta\tau_{\text{in},0}^4 C_{\text{in},0}/F_3 \quad (\text{A2l})$$

$$k_{22} = 1 \quad (\text{A2m})$$

where  $F_i$  ( $i = 1 - 4$ ) are

$$F_1 = (1 + 2\beta/\tau_{\text{in},0}^2)^2 + 16\beta^2 C_{\text{in},0}^2 \quad (\text{A3a})$$

$$F_2 = (2\beta + \tau_{\text{in},0}^2)^2 - 16\beta^2 \tau_{\text{in},0}^4 C_{\text{in},0}^2 \quad (\text{A3b})$$

$$F_3 = \tau_{\text{in},0}^2 + 2\beta(1 + 4\tau_{\text{in},0}^4 C_{\text{in},0}^2) \quad (\text{A3c})$$

$$F_4 = (2\beta + \tau_{\text{in},0}^2)^2 + 16\beta^2 \tau_{\text{in},0}^4 C_{\text{in},0}^2. \quad (\text{A3d})$$

The modulator transfer function (5a)–(5e) is also linearized in terms of the small fluctuations in the pulse parameters as

$$\Delta A_{\text{out}} = \Delta A_{\text{in}} \quad (\text{A4a})$$

$$\Delta\tau_{\text{out}} = \frac{\Delta\tau_{\text{in}}}{(1 + 2\mu\tau_{\text{in},0}^2)^{3/2}} \quad (\text{A4b})$$

$$\Delta C_{\text{out}} = \Delta C_{\text{in}} \quad (\text{A4c})$$

$$\Delta\kappa_{\text{out}} = \Delta\kappa_{\text{in}} - \frac{4\mu C_{\text{in},0}\tau_{\text{in},0}^2}{1 + 2\mu\tau_{\text{in},0}^2} \Delta\xi_{\text{in}} \quad (\text{A4d})$$

$$\Delta\xi_{\text{out}} = \frac{\Delta\xi_{\text{in}}}{1 + 2\mu\tau_{\text{in},0}^2}. \quad (\text{A4e})$$

The subscript in, 0 indicates that the quantity is that of the stationary solution at the entrance of filter and modulator.

#### REFERENCES

- [1] J. Nagel, "Fiber issues for system deployment," in *Proc. Optical Fiber Communication'2001*, Anaheim, CA, 2001, Paper TuD1.
- [2] N. J. Smith, F. M. Knox, N. J. Doran, K. J. Blow, and I. Bennion, "Enhanced power solitons in optical fibers with periodic dispersion management," *Electron. Lett.*, vol. 32, pp. 54–55, 1996.
- [3] M. Suzuki, I. Morita, N. Edagawa, S. Yamamoto, H. Taga, and S. Akiba, "Reduction of Gordon–Haus timing jitter by periodic dispersion compensation in soliton transmission," *Electron. Lett.*, vol. 31, pp. 2027–2028, 1995.
- [4] A. Hasegawa, Y. Kodama, and A. Maruta, "Recent progress in dispersion managed soliton transmission technologies," *Optic. Fiber Technol.*, vol. 3, pp. 197–213, 1997.
- [5] S. K. Turitsyn, "Breathing self-similar dynamics and oscillatory tails of the chirped dispersion-managed soliton," *Phys. Rev. E*, vol. 58, pp. 1256–1259, 1998.
- [6] I. Morita, K. Tanaka, N. Edagawa, and M. Suzuki, "40 Gbit/s single channel soliton transmission over 10 200 km without active inline transmission control," in *Proc. Eur. Conf. Optical Communications'98*, Madrid, Spain, 1998, Postdeadline Papers, pp. 49–51.
- [7] D. Leguen, S. Delburgo, M. L. Moulinard, D. Grot, M. Henry, F. Favre, and T. Georges, "Narrow band 1.02 Tbit/s ( $51 \times 20$  Gbit/s) soliton DWDM transmission over 1000 km of standard fiber with 100 km amplifier spans," in *Proc. Optical Fiber Communication'99*, San Diego, CA, 1999, Postdeadline Papers, PD-4.
- [8] P. V. Mamysheva and N. A. Mamysheva, "Pulse-overlapped dispersion-managed data transmission and intrachannel four-wave mixing," *Opt. Lett.*, vol. 24, pp. 1454–1456, 1999.
- [9] R. J. Essiambre, B. Mikkelsen, and G. Raybon, "Intrachannel cross phase modulation and four wave mixing in high speed TDM systems," *Electron. Lett.*, vol. 35, pp. 1576–1578, 1999.
- [10] M. Nakazawa, E. Yamada, H. Kubota, and K. Suzuki, "10 Gbit/s soliton data transmission over one million kilometers," *Electron. Lett.*, vol. 27, pp. 1270–1272, 1991.
- [11] M. Matsumoto, "Time-domain transmission control of dispersion-managed soliton," *Electron. Lett.*, vol. 34, pp. 2155–2157, 1998.
- [12] S. Waiyapot and M. Matsumoto, "Stability analysis of dispersion-managed solitons controlled by synchronous amplitude modulator," *IEEE Photon. Technol. Lett.*, vol. 11, pp. 1408–1410, Nov. 1999.
- [13] A. Tonello, A. D. Capobianco, S. Wabnitz, O. Leclerc, B. Dany, and E. Pincemin, "Stability and optimization of dispersion-managed soliton control," *Opt. Lett.*, vol. 25, pp. 1496–1498, 2000.
- [14] E. Pincemin, O. Audouin, B. Dany, and S. Wabnitz, "Stability of synchronous intensity modulation control of 40-Gb/s dispersion-managed soliton transmission," *J. Lightwave Technol.*, vol. 19, pp. 624–635, May 2001.
- [15] B. Dany, P. Brindel, O. Leclerc, and E. Desurvire, "Transoceanic  $4 \times 40$  Gbit/s system combining dispersion-managed soliton transmission and new 'black-box' in-line optical regeneration," *Electron. Lett.*, vol. 35, pp. 418–419, 1999.
- [16] B. Dany, P. Brindel, E. Pincemin, D. Rouvillain, and O. Leclerc, "Recovered efficiency of filter control in dispersion-managed solitons for optical regeneration applications: Analysis and experimental validation," *Opt. Lett.*, vol. 25, pp. 793–795, 2000.

- [17] A. Sahara, T. Inui, T. Komukai, H. Kubota, and M. Nakazawa, "40-Gb/s RZ transmission over transoceanic distance in a dispersion managed standard fiber using a new inline synchronous modulation method," *IEEE Photon. Technol. Lett.*, vol. 12, pp. 720–722, June 2000.
- [18] A. Sahara, T. Inui, T. Komukai, H. Kubota, and M. Nakazawa, "40-Gb/s RZ transmission over a transoceanic distance in a dispersion managed standard fiber using a modified inline synchronous modulation method," *J. Lightwave Technol.*, vol. 18, pp. 1364–1373, Oct. 2000.
- [19] A. Sahara, H. Kubota, and M. Nakazawa, "The tolerance of the strength of dispersion map in the dispersion managed soliton system with the synchronous modulation," in *Materials ROSC Workshop*, Kyoto, Japan, Nov. 2000.
- [20] M. J. Holmes, D. L. Williams, and R. J. Manning, "Highly nonlinear optical fiber for all optical processing application," *IEEE Photon. Technol. Lett.*, vol. 7, pp. 1045–1047, Sept. 1995.
- [21] T. Okuno, M. Onishi, T. Kashiwada, S. Ishikawa, and M. Nishimura, "Silica-based functional fibers with enhanced nonlinearity and their application," *IEEE J. Select. Topics Quantum Electron.*, vol. 5, pp. 1385–1391, Sept./Oct. 1999.
- [22] D. Anderson, "Variational approach to nonlinear pulse propagation in optical fibers," *Phys. Rev. A*, vol. 27, pp. 3135–3145, 1983.
- [23] I. Gabitov and S. K. Turitsyn, "Breathing solitons in optical fiber links," *JETP Lett.*, vol. 63, no. 10, pp. 863–868, 1996.
- [24] S. Waiyapot and M. Matsumoto, "Jitter and stability analysis of an actively mode-locked dispersion-managed fiber laser," *Opt. Commun.*, vol. 188, pp. 167–180, 2001.
- [25] J. Kumasako, M. Matsumoto, and S. Waiyapot, "Linear stability analysis of dispersion-managed solitons controlled by filters," *J. Lightwave Technol.*, vol. 18, pp. 1064–1068, 2000.
- [26] M. Matsumoto, "Analysis of optical regeneration utilizing self-phase modulation in a highly nonlinear fiber," *IEEE Photon. Technol. Lett.*, vol. 14, pp. 319–321, Mar. 2002.
- [27] S. K. Turitsyn, E. G. Shapiro, and V. K. Mezentsev, "Dispersion-managed solitons and optimization of the dispersion management," *Opt. Fiber Technol.*, vol. 4, pp. 384–402, 1998.

**S. Waiyapot**, photograph and biography not available at the time of publication.

**S. K. Turitsyn**, photograph and biography not available at the time of publication.

**V. K. Mezentsev**, photograph and biography not available at the time of publication.